

## The Li Insertion/Extraction Characteristics of Amorphous Silicon Thin Films

T. L. Kulova, A. M. Skundin,<sup>+</sup> Yu. V. Pleskov, O. I. Kon'kov,\*  
E. I. Terukov,\* and I. N. Trapeznikova\*

Frumkin Institute of Physical Chemistry and Electrochemistry, RAS  
31, Leninskii prospect, 119991 Moscow, Russia

\*Ioffe Physico-Technical Institute, RAS  
26, ul. Politekhnikeskaya, 124021 St. Petersburg, Russia

Original scientific paper  
Received: September 12, 2006  
Accepted: December 13, 2006

Amorphous hydrogenated silicon (a-Si:H) is known to be a perspective material for negative electrodes of modern lithium-ion batteries. The electrochemical lithium insertion into thin-film a-Si:H electrodes is studied using chronopotentiometry, cyclic voltammetry (CV), and electrochemical impedance spectroscopy (EIS). The electrodes were grown on stainless-steel substrates by glow discharge at the temperature of  $T = 100$  and  $250$  °C. The insertion capacity of the films deposited at  $250$  °C is higher than that of the equally thick films deposited at  $100$  °C. The increase in the film thickness involves the drastic decrease of the insertion capacity during the potential cycling. An equivalent circuit is suggested for the lithium insertion to the electrodes, which comprises electrolyte resistance and three RC-chains in series, each chain being a parallel connection of a resistance and a constant-phase element, which relate to charge transfer at the silicon/electrolyte interface, charge transport in the passive film on silicon, and the lithium diffusion into the silicon bulk. With the potential cycling in progress, the most significant changes are observed in the chain relating to the passive film. The Li diffusion coefficient in a-Si:H is estimated from data of CV and EIS. It equals  $D = 4 \cdot 10^{-13}$  and  $10^{-13}$   $\text{cm}^2 \text{s}^{-1}$  for electrodes synthesized at a temperature of  $100$  and  $250$  °C, respectively.

### Key words:

Amorphous silicon, thin films, lithium insertion, diffusion coefficient, chronopotentiometry, electrochemical impedance spectroscopy

## Introduction

Lithium-ion batteries are well-known to be the most promising because of their highest discharge capacity and working voltage. In fact, the creation of modern portable IT electronic appliances such as cellular phones, notebooks, digital cameras, and camcorders was due to the development of lithium-ion batteries. Recently an interest in lithium-ion microbatteries, namely thin-film batteries was increased in the connection with the development of smart cards, MEMS etc.

Negative electrodes of modern lithium-ion batteries used to be made of carbonaceous materials, e.g. of graphite. The maximal lithium amount, which can be intercalated into graphite, comes to  $Q = 0.372 \text{ Ah g}^{-1}$ , which corresponds to the stoichiometry of  $\text{LiC}_6$ . Meanwhile, silicon is able to form the compounds with the general formula  $\text{Li}_x\text{Si}$ , where  $x$  can be as high as 4.4, i.e. the capacity of the silicon electrode can amount to  $4.2 \text{ Ah g}^{-1}$  ( $9.3 \text{ Ah dm}^{-3}$ ). Unfortunately, the Li incorporation into

silicon (like numerous other matrices) involves almost a three-fold increase in its specific volume, which results in the disintegration of crystalline Si electrodes.<sup>1,2</sup> It was found recently that, unlike crystalline silicon, amorphous Si (used mainly as thin films) does not disintegrate upon lithium insertion. By now numerous papers devoted to lithium insertion into amorphous silicon were published; however, the literature data are scarce and rather contradictory.<sup>3–15</sup> The latter fact must be mainly due to the differences in the procedures of sample preparation. In particular, the amorphous silicon films were grown on molybdenum<sup>3</sup> and porous nickel<sup>4</sup> substrates by chemical deposition from  $\text{Si}_2\text{H}_6$  vapor; on nickel foil, by vacuum evaporation;<sup>5,8–11</sup> on copper foil, by magnetron sputtering;<sup>6,7,13</sup> on silicon wafers by magnetron sputtering,<sup>14</sup> and on stainless steel, by pulsed laser deposition.<sup>15</sup>

In this work we aimed at studying of lithium insertion into hydrogenated amorphous silicon (a-Si:H) thin films. For the sake of comparison, some experiments were carried out with the crystalline silicon samples.

<sup>+</sup>Corresponding author. E-mail: askundin@mail.ru

## Experimental

### Manufacturing hydrogenated amorphous silicon films

Thin films of amorphous hydrogenated silicon (a-Si:H) were synthesized from  $\text{SiH}_4$  by a method of rf glow discharge.<sup>16</sup> It was proved in the cited work that thus produced a-Si:H films are X-ray-amorphous. The substrates were 150  $\mu\text{m}$ -thick stainless steel sheets. The synthesis was conducted at temperatures of 100 and 250 °C. The increase of the synthesis temperature resulted in the decrease of the residual hydrogen content in the films from ~12 to ~8 at. %. Additionally, the character of the silicon-hydrogen bonds may change as well. The density of the material obtained at temperatures of 100 and 250 °C was equal to  $\rho = 2.0$  and  $2.2 \text{ g cm}^{-3}$ , respectively whereas the density of crystalline silicon is  $\rho = 2.33 \text{ g cm}^{-3}$ . The thickness of the a-Si:H films (from  $\delta = 0.25$  to  $1.35 \mu\text{m}$ ) was controlled by varying film deposition time.

The crystalline silicon electrodes were cut from a commercial 0.3 mm-thick wafer with a mirror-polished surface.

### Electrochemical measurements

The processes of lithium insertion and extraction were investigated by galvanostatic method, cyclic voltammetry (CV), and electrochemical impedance spectroscopy (EIS). The measurements were performed in glass cells in a large excess of electrolyte or in Teflon cells with tightly assembled electrodes. Performing the experiments in a glass cell allows us to observe variations in electrode appearance in the course of its cycling. The Teflon cells were designed similarly to real lithium-ion batteries. The visible surface area of the working electrodes was equal to  $A = 0.6$  or  $0.4 \text{ cm}^2$  for amorphous silicon;  $0.6 \text{ cm}^2$ , for crystalline silicon. The auxiliary and the reference electrodes were made of lithium metal that was rolled up onto a nickel gauze. The electrolyte volume in the glass cells with non-separated anodic and cathodic compartments was ca.  $3 \text{ cm}^3$ . The electrodes in the Teflon cells were separated by a 25  $\mu\text{m}$ -thick porous polypropylene film "PORP" (NPO Ufim, Moscow) impregnated with the electrolyte. The electrolyte was a  $1 \text{ mol dm}^{-3}$   $\text{LiClO}_4$  solution in a propylene carbonate-dimethoxyethane mixture ( $\psi = 7:3$ ). The electrolyte humidity measured by Fischer coulometric titration (684 KF-Coulometer, "Metrohm," Switzerland) did not exceed  $w = 50 \cdot 10^{-6}$ . The cells were assembled and filled with the electrolyte in a glove box with an argon atmosphere.

The galvanostatic charge–discharge curves were registered using a homemade multichannel

computerized instrument for potential cycling. The charge current (cathodic for this particular experiment) and the discharge current (anodic) were equal to  $70 \mu\text{A}$ . The cyclic voltammograms (CVA) were registered using an EL-2 potentiostat designed and manufactured in the Frumkin Institute of Electrochemistry, Russian Academy of Sciences, Moscow. The potential scan rate ( $\nu$ ) covered the range from 50 to  $900 \mu\text{V s}^{-1}$ .

The impedance spectra were registered over the 25 mHz–100 kHz frequency range, using a Solartron frequency analyzer (model 1255) and a Solartron electrochemical interface (model 1286). The amplitude of the applied voltage was  $U = 10 \text{ mV}$ . The impedance spectra were taken at several preset potential values during the first and second runs of the charge–discharge curves. Additionally, the impedance spectra were taken at some chosen potentials in the course of prolonged cycling (up to 230 cycles).

Based on preliminary speculative analysis of the impedance spectra, some equivalent circuit was suggested. Its elements were found by the minimizing of the mean-square deviation of the measured impedance modulus from that calculated for a suggested equivalent circuit; in these calculations, adopted software<sup>17</sup> was used.

## Results and discussion

### Lithium insertion into crystalline silicon

The initial open-circuit potential of crystal silicon electrodes was ca. 2.2 V; it is more likely than not determined by oxygen-containing groups present at the silicon surface. During the first cathodic polarization half-cycle, the potential dropped to ca. 0.03 V; then it became more positive and slowly reached its steady-state value ranging from 0.09 to 0.12 V (Fig. 1). At this potential, some steady-state process occurred (in all probability, electrolyte re-

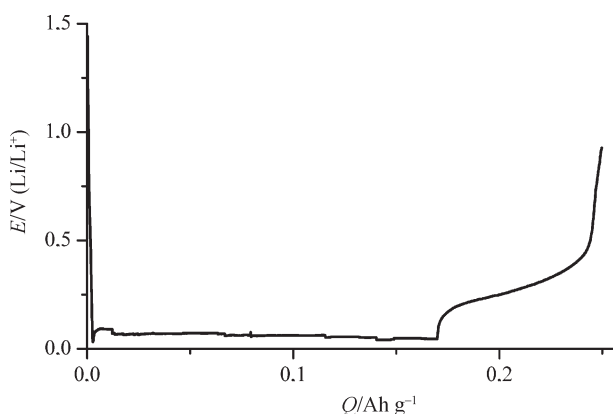


Fig. 1 – Cathodic (charge) and anodic (discharge) galvanostatic curves of the 1<sup>st</sup> cycle for crystalline silicon electrode.

duction) in addition to the lithium insertion. When the current was reversed, the anodic galvanostatic curves showed a plateau at the 0.2–0.3 V potential range, which corresponded to extraction of the incorporated lithium. Largely, the shape of the curves is characteristic of silicon electrode (see e.g. 1<sup>8</sup>). We recall that the cathodic behavior of silicon differs from that of carbonaceous materials. Indeed, at the graphite surface the electrolyte is reduced in the potential range 1.2–0.7 V, thus yielding passive film (so-called solid electrolyte interface, SEI) at the electrode surface. The SEI that possesses Li<sup>+</sup>-conductivity hampers the further electrolyte reduction during the following potential cycling. With the silicon electrodes, no plateau at 1.2–0.70 V in the cathodic run of the charge-discharge curves was observed in the first and subsequent cycles. Thus, the electrolyte is not subjected to reduction in this potential range. Yet one can say with a fair degree of confidence that the reduction process proceeds at the potentials close to the lithium electrode potential; hence, the current in the cathodic plateau near 0.1 V is consumed in part for the sustaining of this very process. This suggestion is corroborated by the fact that the charge  $Q_c$  consumed during the cathodic half-cycle exceeds markedly the charge  $Q_a$  released during the anodic half-cycle. The difference  $Q_c - Q_a$  corresponds to a loss related to the so-called irreversible capacity  $Q_{irr}$ . During the first cathodic half-cycle,  $Q_{irr}$  is consumed for formation of gaseous and soluble products as well as for SEI formation. It is the last process that eliminates electrolyte reduction in following cycles. That is why  $Q_{irr}$  at the second and following cycles is much less than that at the first cycle. The electrolyte reduction in following cycles is possible due to defectness of SEI.

As we have already mentioned in the Introduction, the lithium insertion and extraction process involves the disintegration of the silicon crystal lattice. The particular character of this disintegration is mainly determined by the method of silicon sample manufacturing. When cycling the potential of the commercial wafer used in this work, only surface destruction (some kind of “etching”) of the silicon plates was observed, and this resulted in the increased surface area (Fig. 2). This process was clearly visualized when using the glass cells. Additionally, the current in the CVA ever increased as the silicon potential was cycling, which also evidences the growing surface area (Fig. 3).

#### Lithium insertion into amorphous silicon films obtained at different temperatures

In order to compare the Li-insertion behavior of a-Si:H films synthesized at different temperatures, galvanostatic measurements at a current of 70

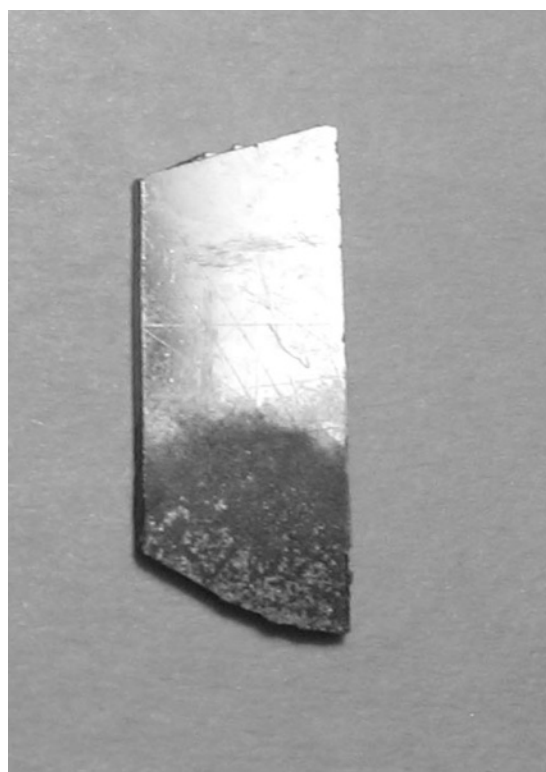


Fig. 2 – Silicon wafer electrode after lithiation with current density  $j = 0.7 \text{ mA cm}^{-2}$  for  $t = 72 \text{ h}$ . The surface that contacted the electrolyte has been etched up; eventually, the wafer disintegrated.

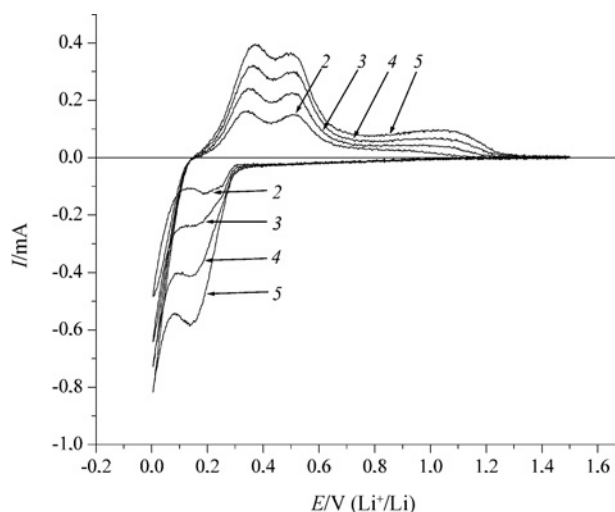


Fig. 3 – Cyclic voltammograms at the electrode made from silicon wafer. Figures near curves are cycle numbers

$\mu\text{A}$  were carried out. Due to the difference in the film thickness, the current density, when calculated per unit silicon mass, was equal to  $I = 700$  and  $1000 \text{ mA g}^{-1}$  for the films deposited at the temperatures of 100 and 250 °C, respectively. All the experiments were conducted in the Teflon cells with a tight assemblage. Fig. 4 demonstrates galvanostatic

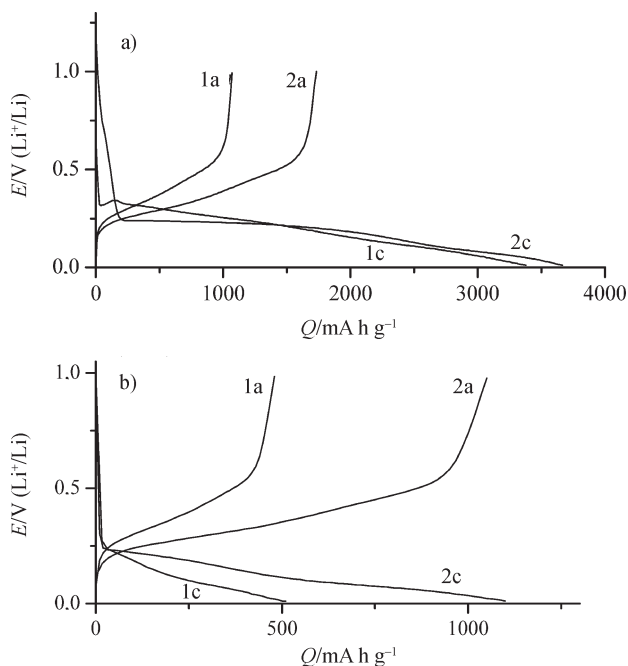


Fig. 4 – (a) Cathodic (1c, 2c) and anodic (1a, 2a) galvanostatic curves of the 1<sup>st</sup> cycle for a-Si:H thin-film electrodes, deposited at the temperatures  $T = 100\text{ }^{\circ}\text{C}$  (1c, 1a) and  $250\text{ }^{\circ}\text{C}$  (2c, 2a). (b) The same for 10<sup>th</sup> cycle.

curves that correspond to the first (Fig. 4a) and tenth (Fig. 4b) cycles. For both films,  $Q_c$  in the first cycle perceptibly exceeds  $Q_a$ , which points to the occurrence of an irreversible process during the first cathodic polarization cycle. In the tenth cycle,  $Q_c$  is virtually equal to  $Q_a$ . This means that the process of lithium insertion-extraction occurs reversibly. By analogy with the behavior of graphite electrodes, one can assume that the irreversible reduction of electrolyte components (mainly of the solvent) during the initial cycles leads to the formation of the above-mentioned SEI. By and large, the curves in Fig. 4 conform to those described in literature.

One can see that the discharge capacity of a-Si:H films that were obtained at a temperature of  $250\text{ }^{\circ}\text{C}$  noticeably exceeds that of the films produced at  $100\text{ }^{\circ}\text{C}$  despite the fact that the current density at the cycling of the films manufactured at  $250\text{ }^{\circ}\text{C}$  was 1.5 times greater than that for the films prepared at  $100\text{ }^{\circ}\text{C}$ . At this point, we cannot say definitely whether it is associated with the different content of residual hydrogen in the films or with some other factors; in particular, the increase of film density with the increase of deposition temperature may point to a change in the microscopic structure of the material.

Some authors<sup>13</sup> described properties of thin amorphous silicon films deposited onto copper substrates using RF magnetron sputtering at room tem-

perature and at 100, 200, and  $300\text{ }^{\circ}\text{C}$ . The films deposited at  $200\text{ }^{\circ}\text{C}$  were found to have the best insertion capability. According to the authors, the good cycleability of the films is due to the proper Si/Cu interdiffusion and minimal film stress. The deposition temperature undoubtedly influences the mechanical properties of the films and their adhesion to substrates. However, it hardly is the sole effect of the deposition temperature.

For the first 8–10 cycles, the discharge capacity very rapidly diminishes from cycle to cycle, the capacity fading being faster for the films synthesized at  $100\text{ }^{\circ}\text{C}$  than for those synthesized at  $250\text{ }^{\circ}\text{C}$ . Then, the rate of decrease in capacity slows down. The question as to why the capacity of the silicon electrodes diminishes during cycling is still unanswered; it is rarely discussed in the relevant literature. It must be emphasized that the literature data on the decrease in the capacity of the amorphous silicon thin-film electrodes is rather contradictory.<sup>3–10,19,20</sup>

#### Effect of film thickness on lithium insertion

Figure 5 presents galvanostatic curves recorded in the first cycle for thin-film a-Si:H electrodes of different thickness; the films were synthesized at  $250\text{ }^{\circ}\text{C}$ . The cycling was performed with current of  $I = 0.07\text{ mA}$  ( $j = 0.175\text{ mA cm}^{-2}$ ), which corresponded to the current densities of 3500, 2030, 1200, and  $610\text{ mA g}^{-1}$  for the 0.25, 0.43, 0.73, and  $1.35\text{ }\mu\text{m}$ -thick films. We see that the character of these curves is the same, and in all cases  $Q_c$  exceeds  $Q_a$  in the first cycle, which evidences the occurrence of some irreversible processes. There is no correlation whatsoever between the  $Q_{irr}$  in the first cycle and the film thickness. However, noteworthy is the marked irreproducibility of the  $Q_{irr}$  values for electrodes with films of the same thickness.

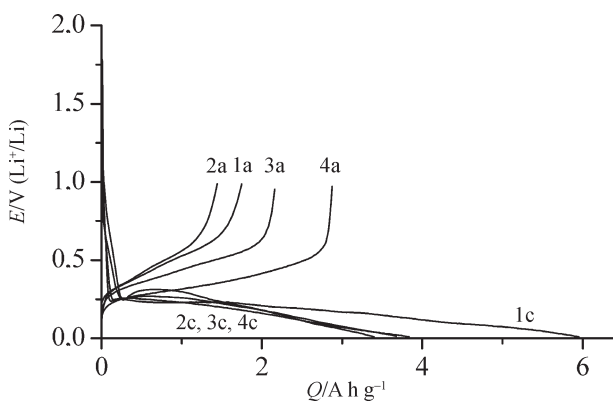


Fig. 5 – Cathodic (1c–4c) and anodic (1a–4a) galvanostatic curves of the 1<sup>st</sup> cycle for a-Si:H thin-film electrodes, deposited at the temperature  $250\text{ }^{\circ}\text{C}$ . Film thickness ( $\delta/\mu\text{m}$ ): 0.25 (1a, 1c); 0.43 (2a, 2c); 0.73 (3a, 3c); 1.35 (4a, 4c).

The dependence of the reversible capacity on film thickness at the same current density calculated per unit visible surface area is of complicated character. In the first cycle, the discharge capacity of thicker films exceeds that of thinner films, which is but logical, because the current density for the thicker films is a few times smaller than that for thinner films. However, as early as by the third cycle, the values of the discharge capacity for the film electrodes of different thickness become identical. This can be explained by the different character of variations in the discharge capacity of the electrodes in the course of their cycling. Fig. 6 illustrates the variations in the discharge capacity of electrodes with films of different thickness during their cycling. Characteristically, the rate of capacity fading of the films of small thicknesses turned out to be lower than that for the 0.73 and 1.35  $\mu\text{m}$ -thick films. Besides, the discharge capacity of electrodes with the films 0.23 and 0.43  $\mu\text{m}$  thick initially (for the first 6–10 cycles) somewhat increases with the cycling in progress, then begins decreasing. The discharge capacity of the electrodes with thicker amorphous silicon films decreases during their cycling beginning with the very first cycle (Fig. 6, insert).

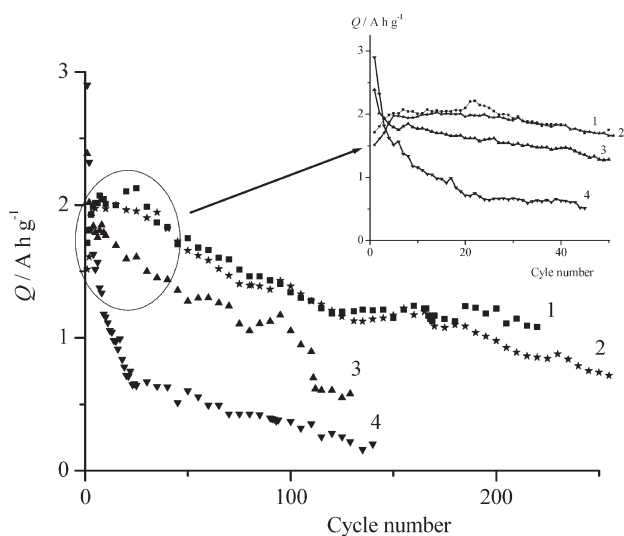


Fig. 6 – Change of the discharge capacity of *a*-Si:H thin-film electrodes, deposited at the temperature 250°C. Film thickness ( $\delta/\mu\text{m}$ ): (1) 0.25; (2) 0.43; (3) 0.73; (4) 1.35. The curves were taken with the current 0.07 mA (insert: the initial segments of the curves)

Why the decay in the discharge capacity accelerates with increasing film thickness we cannot yet explain. It may result from trivial destruction (or exfoliation from the substrate) of thicker films (this reason is noted also in ref. 13). Indeed, once the cells were disassembled after prolonged cycling, the films 0.73 and 1.35  $\mu\text{m}$  thick appeared virtually

detached from their substrates. The thinner films underwent only partial destruction.

The electrodes prepared from thin-film amorphous silicon of different thickness were cycled at identical current density, as calculated per mass of the active substance: 3500  $\text{mA g}^{-1}$ . Here, the current density calculated per unit visible surface area was equal to  $j = 0.175, 0.30, 0.51,$  and  $0.97 \text{ mA cm}^{-2}$  for the films  $\delta = 0.25, 0.43, 0.73,$  and  $1.35 \mu\text{m}$  thick. During the cycling, the discharge capacity of thinner films exceeded that of thicker films beginning with the first cycle. The low values of the discharge capacity for the electrodes with thicker films can be attributed to a significant non-uniformity of lithiation over the film thickness. The nonuniformity of lithium distribution over the electrode thickness increases with the current density as calculated per unit visible surface area of the electrodes. As the cycling proceeds further, the decrease in the discharge capacity for thicker films was more pronounced than that for thinner films, which is due to a trivial reason, in particular, the exfoliation of amorphous silicon films from the substrate.

#### Cyclic voltammetry of *a*-Si:H thin-film electrodes

Figure 7 shows CVAs for the electrodes synthesized at the temperatures of 100 and 250 °C. These experiments were also conducted in Teflon

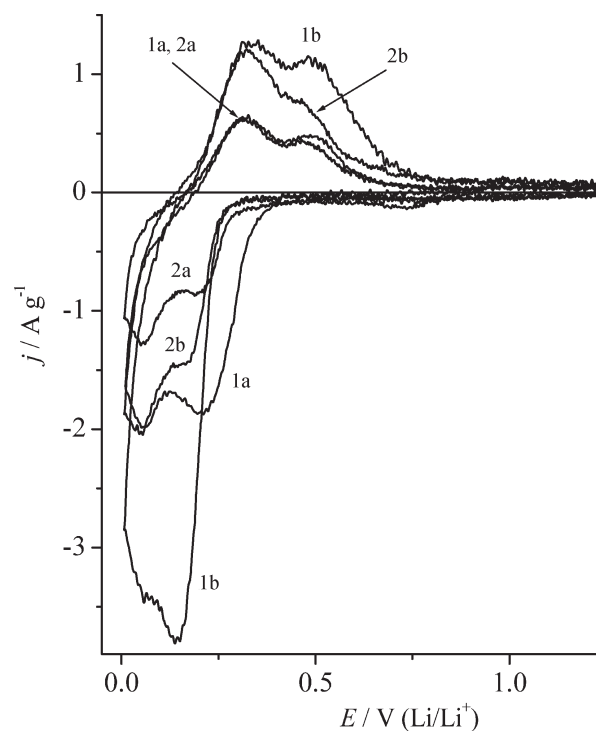


Fig. 7 – Cyclic voltammograms for *a*-Si:H thin-film electrodes for the 1<sup>st</sup> cycle (1a, 1b) and 2<sup>nd</sup> cycle (2a, 2b). The films were deposited at the temperatures 100 °C (1a, 2a) and 250 °C (1b, 2b). The potential scan rate is  $10^{-4} \text{ V s}^{-1}$ .

cells with a tight assemblage. The curves were recorded at a rather slow potential scan rate of  $10^{-4}$  V  $s^{-1}$ . As seen in Fig. 7, the CVAs agree with the galvanostatic curves shown in Fig. 4.

With both electrodes, the charge  $Q_c$  consumed during the cathodic run of the curve exceeds markedly the charge  $Q_a$  released during the anodic run in the first cycle, which also points to the occurrence of irreversible processes during the first cathodic polarization. Two cathodic peaks at the potentials of about 0.20 and 0.06 V reflect the process of lithium insertion. However, irreversible processes that are probably related to the above-mentioned electrolyte reduction camouflage this reversible process. These cathodic peaks correspond to the anodic peaks at the potentials of  $\sim 0.32$  and 0.49 V in the reverse run of the CVAs, which reflect the process of lithium extraction. Almost the same results were reported also in Refs. 5–7, 10.

The raising of the potential scan rate leads to an increase in the height of the peaks corresponding to the lithium insertion and extraction. The peaks turn smoother, the cathodic peaks shift to negative potentials while the anodic peaks to positive potentials (Fig. 8). The current in the first anodic peak (at  $E \sim 0.32$  V) appeared to be a linear function of  $\sqrt{v}$  ( $v$  is the potential scan rate); the line strikes the origin, which indicates that the process of lithium insertion–extraction is under the diffusion control. Such dependence allows calculating the lithium diffusion coefficient  $D_{Li}$ . The calculation requires knowledge of the concentration dependence of

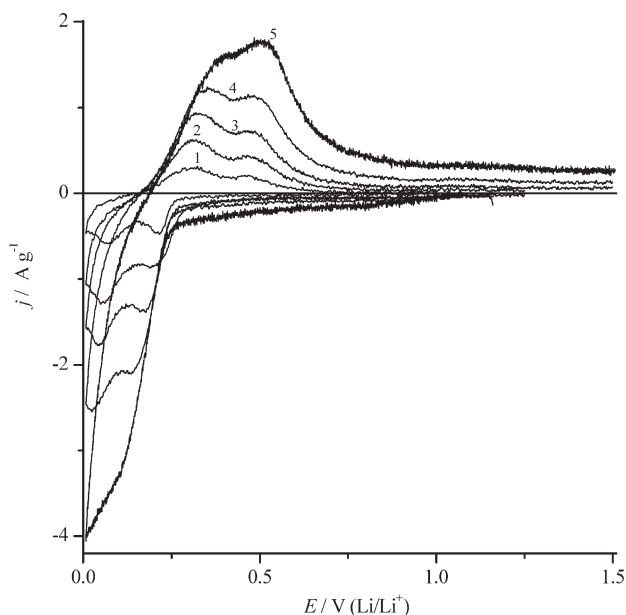


Fig. 8 – Cyclic voltammograms for a-Si:H thin-film electrodes deposited at temperature 100 °C. The potential scan rate ( $V s^{-1}$ ): (1)  $5 \cdot 10^{-5}$ ; (2)  $10^{-4}$ ; (3)  $2 \cdot 10^{-4}$ ; (4)  $4 \cdot 10^{-4}$ ; (5)  $9 \cdot 10^{-4}$ . The curves are recorded during the 3<sup>rd</sup>, 4<sup>th</sup>, 5<sup>th</sup>, 6<sup>th</sup>, and 7<sup>th</sup> cycles.

the potential, which in the present case is non-Nernstian. The interrelation between the potential  $E$  and the lithium concentration  $c$  can be found from a quasi-equilibrium discharging curve (that is, the dependence of  $E$  on the passed charge  $Q$ ). The  $E$  vs.  $Q$  dependence is nearly linear over a wide potential range, with the proportionality coefficient  $dE/dQ = 2.8 \cdot 10^{-5} \Omega g s^{-1}$ .

Evidently,

$$dQ = dc n F/\rho \quad (1)$$

where  $\rho$  is the density of amorphous silicon ( $\rho = 2.2 g cm^{-3}$ ).

With due account for Eq. (1), the expression for calculating  $D_{Li}$  can be written as

$$D_{Li} = \frac{5}{\rho c F} \frac{dF}{dQ} \left( \frac{dj}{d\sqrt{v}} \right)^2 \quad (2)$$

(instead of the traditional formula

$$D_{Li}^{1/2} = j_p / (2.69 \cdot 10^5 n^{3/2} c v^{1/2}), \quad (3)$$

which is based on the Nernstian dependence of  $E$  on  $c$ ). Here  $j_p$  is the current density in the CVA peak,  $n$  is the number of electrons transferred per one diffusing particle, the concentration  $c$  was calculated by integrating the cathodic curve recorded at a rather low potential scan rate. For the a-Si:H thin-film electrodes prepared at 100 and 250 °C,  $D_{Li}$  came to  $9 \cdot 10^{-13}$  and  $4 \cdot 10^{-13} cm^2 s^{-1}$ , respectively. This may be due to the increase in the film density (which is likely to reflect a change in the microscopic structure of the material) caused by the increase in the deposition temperature, as suggested above. (No reliable data on the lithium diffusion coefficient in amorphous or crystalline silicon is at hand, to our knowledge. An attempt to measure the lithium diffusion coefficient in the amorphous silicon films using the potential-step chronoamperometry method was made.<sup>11</sup> However, the authors concluded that the rate-determining step in their experiments was not the lithium diffusion, so the figures obtained are no more than apparent). The increase in the Li diffusion coefficient must facilitate the lithium diffusion in the a-Si:H bulk, hence, improve the electrochemical properties (in particular, the insertion capacity) of the lithium electrode.

#### The impedance studies of a-Si:H thin-film electrodes

It is but surprising why such an informative method of investigation as electrochemical impedance spectroscopy (EIS) has never been invoked for investigating lithium insertion into silicon. (The only exceptions are the works devoted to studying

silicon/carbon composites<sup>18,21,22</sup> and silicon/poly-pyrrole composites.<sup>19</sup>)

In the present work, only electrodes prepared at 250 °C were used for EIS study. As one can see from Fig. 4, the galvanostatic cathodic charge curve could be conveniently divided into two segments. The first sharply descending from 1.5 to ca. 0.25 V, refers to the processes of electrical double layer charging and the slow reduction of the electrolyte or impurities therein. The slope of this segment of the curve corresponds to a full differential capacitance of 70–75 mF cm<sup>-2</sup>; and this certainly exceeds the electrical double layer capacitance. The second, gently sloping, segment covers the potential range from 0.25 to 0.0 V, and it relates to the lithium insertion. Figure 9 presents typical Nyquist plots corresponding to the first (Fig. 9a) and the second (Fig. 9b) segments. These data were obtained during the first cathodic polarization of a freshly prepared electrode. Qualitatively, these plots resemble those reported for the silicon-powder electrodes.<sup>19,21</sup> Apparently, the spectra measured in the first and second segments of the cathodic galvanostatic curve have similar appearance. Indeed, they both show a somewhat depressed semicircle in their high-frequency domain, the center of which lies below the abscissa axis. The low-frequency segment of the plot measured at 380 mV is nearly a straight

line with a slope of 47°. While the low-frequency segment of the plot measured at 25 mV (where the lithium incorporation can occur) may be thought of as a part of a large-radius semicircle.

The impedance spectra measured during the second charging-discharging cycle are similar to those obtained during the first cycle.

With the cycling in progress, the electrodes' capacity decreases (Fig. 10) and the appearance of the complex-plane (Nyquist) plots of the impedance spectra changes.\* After prolonged cycling, the high-frequency semicircle eventually splits in two (Fig. 11). Note, that the Nyquist plots with two semicircles in their high-frequency domain were observed.<sup>18</sup>

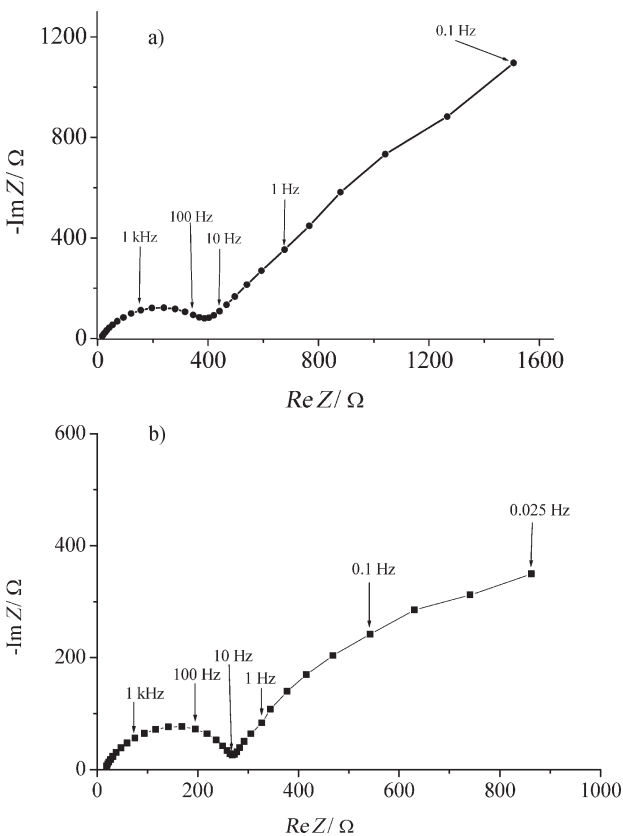


Fig. 9 – Nyquist plots, taken during the 1<sup>st</sup> cycle at the potential 380 mV (a) and 25 mV (b).

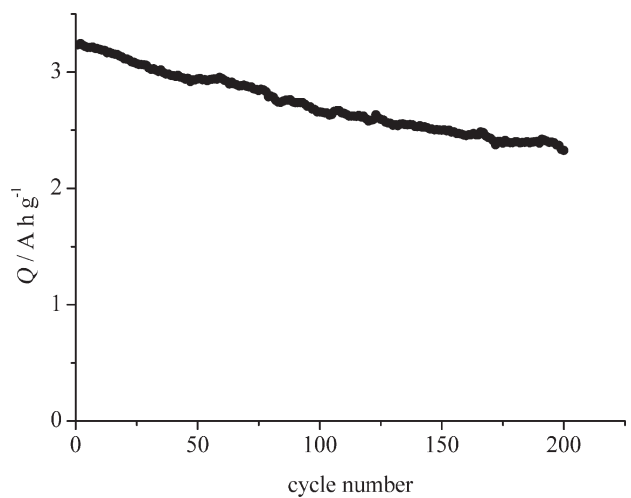


Fig. 10 – Change of the discharge capacity of a-Si:H electrodes with thickness 0.25 μm (improved batch)

From the shape of the plots measured at different potentials and for different cycle numbers, a generalized equivalent circuit was derived. The equivalent circuit comprises four chains connected in series (Fig. 12). The first one is the electrolyte resistance  $R_e$  (more strictly,  $R_e$  includes all ohmic resistances in the system, other than the resistances of electrical double layers and diffusion regions). The second chain is a parallel combination of a resistance ( $R_1$ ) and a constant-phase element (CPE)  $Q_1$ . This combination relates to the high-frequency semicircle in the complex-plane plots of the impedance spectra. The third chain is a similar combination of a resistance ( $R_2$ ) and a constant-phase element ( $Q_2$ ). Finally, the fourth chain is a parallel combination of a resistance ( $R_3$ ) and a con-

\* In the present work two batches of electrodes prepared at 250 °C were used. The second batch was manufactured with some special treatment of substrate surfaces. This results in better performance of the electrodes from this batch as compared with the electrodes from the first one. The EIS studies were carried out with the electrodes from the second (improved) batch. Fig. 10 corresponds to these very electrodes, by contrast to Fig. 6.

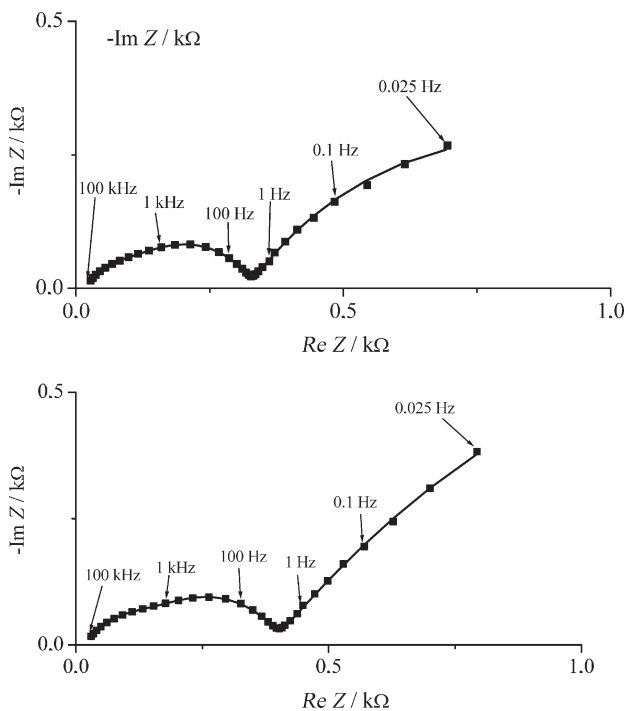


Fig. 11 – Nyquist plots, taken during 126<sup>th</sup> (a) and 220<sup>th</sup> (b) cycles at the potential 10 mV.

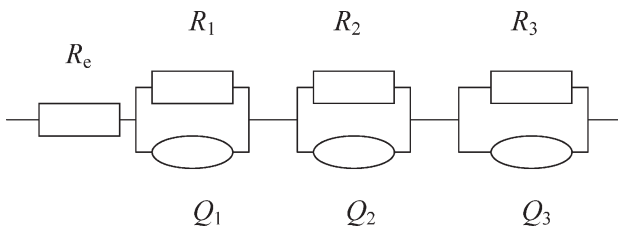


Fig. 12 – The equivalent circuit of the thin-film electrodes

stant-phase element ( $Q_3$ ). This chain corresponds to the low-frequency segments of the impedance spectra. Each CPE element is characterized by a power ( $n_1$ ,  $n_2$ , and  $n_3$ ).

The power  $n_1$  is always close to 1; hence, to a good approximation  $Q_1$  can be considered as a frequency-independent capacitance  $C_1$ , rather than a CPE. In the potential domain 0–200 mV, where the lithium insertion occurs, this capacitance practically is potential-independent (its variation falls within the experimental scatter) and varies but insignificantly as the potential cycling occurs, falling in the 15–25  $\mu\text{F cm}^{-2}$  range. We believe that  $C_1$  is the electrical double layer capacitance that relates to the silicon/electrolyte or silicon/passive film interface. Then the resistance  $R_1$  is the charge transfer resistance for the lithium intercalation process at either of the interfaces.

The third chain in the equivalent circuit can be related to the charge transfer through the passive film. The power  $n_2$  in the CPE  $Q_2$  is equal to 0.65–0.7.

Finally, the fourth chain in the equivalent circuit in all probability represents the lithium diffusion in the amorphous silicon bulk. The power  $n_3$  of the CPE  $Q_3$  in most cases is close to 0.5. We emphasize that reasonable values of CPE  $Q_3$  can be calculated only for the data related to the second segment of the cathodic charging curve, i.e. only for the cases of possible lithium insertion.

The powers  $n_2$  and  $n_3$  somewhat decrease during the potential cycling. It may be suggested that the nature of both  $Q_2$  and  $Q_3$  is determined either by diffusion processes (the lithium diffusion in the passive film and silicon bulk, respectively), or the silicon and/or the passive film surface geometrical structure, or both. It is known that the phase shift for the impedance of an “ideally rough” electrode surface that can be conditionally simulated by a porous layer is half that for the same processes occurring at an “ideally smooth” surface (see e.g. ref. 23). For example, for a rough surface the phase shift for the impedance relating to its double-layer capacitance equals  $\pi/4$ , while the phase shift for the impedance describing the diffusion to this surface (or in a porous layer) is  $\pi/8$  in an ideal case. For realistic combinations of the two factors (the diffusion and surface roughness), the power in CPEs can differ from 0.5.

At the initial stages of potential cycling, the impedance corresponding to the third chain in the equivalent circuit ( $R_2Q_2$ ) is small as compared to that corresponding to its second part ( $R_1Q_1$ ); therefore, only one semicircle (related to  $R_1Q_1$ ) can be seen in the complex-plane plots of impedance spectra. With the cycling in progress, the impedance of the  $R_2Q_2$ -combination increases, probably because of the passive film ageing, in particular, thickening or changing of its composition and structure. This results in the appearance of the second semicircle, even if not well resolved.

The Warburg constant, calculated by Eq. (4) (see below), slightly decreases as the cycling continues. This minor decrease may be assigned to loosing surface.

To a first approximation, the initial part of the low-frequency segment in the Nyquist plots can be considered as a straight line. In this case, the lithium diffusion coefficient can be calculated from the measured values of the impedance imaginary component ( $\text{Im } Z$ ).

The frequency dependence of  $\text{Im } Z$  can be expressed as follows:

$$-\text{Im } Z = W / \sqrt{4\pi f} \quad (4)$$

where  $W$  is the Warburg constant,  $f$  is the ac frequency.

The Warburg constant, in its turn, is related to the dependence of the equilibrium potential  $E$  on the concentration of the diffusing species (lithium, in our case)  $c$ :

$$W = \frac{-dE/dc}{F\sqrt{D}} \quad (5)$$

By combining equations (1), (4) and (5), we obtained the following expression for the diffusion coefficient:

$$D = \frac{(dE/dQ)^2}{2\rho^2 W^2} = \frac{(dE/dQ)^2}{4\pi f \rho^2 (\text{Im } Z)^2} \quad (6)$$

The diffusion coefficient calculated by Eq.(6) for the potential of 10 mV equals  $3 \cdot 10^{-13} \text{ cm}^2 \text{ s}^{-1}$ . This value largely agrees with that estimated from the CV measurements for the electrodes from a different batch. It is not surprising that the diffusion coefficient of lithium in silicon, like in carbonaceous materials, can depend on potential, that is, on the lithiation degree. Then the diffusion coefficient determined from the CVAs must be an average (effective) quantity.

The part of the Nyquist plot corresponding to the lowermost frequencies declines from a straight line obeying the Warburg impedance law for semi-infinite diffusion. This declination can be explained by that at such low frequencies the film thickness becomes comparable with the diffusion length. In this case, the CPE  $Q_3$  could be considered as a bounded CPE. The transition from the semi-infinite to bounded diffusion is determined by inequality

$$f < \frac{\sigma^2 (dE/dQ)^2}{\pi \delta^2 \rho^2 D} \quad (7)$$

Here  $\sigma$  is the silicon conductance,  $\delta$  is the film thickness. An estimation by using equation (7) shows that the transition from semi-infinite to bounded diffusion occurs at a frequency of ca. 0.1 Hz. This agrees with the experimental data.

The proposed equivalent circuit is but an approximation. Indeed, an electrode represented by this equivalent circuit should pass constant current infinitely long; in accord with the physical meaning of the chain  $R_3Q_3$ , this current must correspond to the lithium diffusion. Meanwhile, the film has finite volume, therefore, on its saturation with lithium the current should cease. Therefore, the proposed equivalent circuit cannot describe the electrode behavior at infra-low frequencies; but it fits the conditions of the present experiments.

The CPE  $Q_2$  refers to the charge transfer through the SEI. It is the finite thickness of the film

that determines the shape of the corresponding part of the Nyquist plot, that is, the specifically distorted semicircle instead of a straight line.

In the initial period of cycling, the impedance of the chain ( $R_2Q_2$ ) is small in comparison with that of the chain ( $R_1Q_1$ ). Therefore, the Nyquist plots reveal only one semicircle that corresponds to this very chain. With the cycling in progress, the impedance of the chain ( $R_2Q_2$ ) increases. This could possibly be caused by the increase in the passive film thickness or modification of the film composition and/or structure (ageing). Eventually, two semicircles, even if not very clearly resolved, appear in the complex-plane plots of the impedance spectra.

Thus, the EIS measurements allowed separating the electrode process into several stages, their preliminary identifying, and determining their quantitative characteristics.

## Conclusion

Lithium insertion into hydrogenated amorphous silicon (a-Si:H) thin films is studied. Recent literature information that, unlike crystalline Si, thin films of amorphous Si are suitable for prolonged cycling is confirmed. The discharge capacity of a-Si:H thin films grown at 250 °C proved to be higher than that of the equally thick films deposited at 100 °C. The discharge capacity of the films deposited at 250 °C was shown to depend on their thickness and on the surface treatment of substrates. Specifically, the capacity fading of thicker films is much higher than that of thinner films. The Li diffusion coefficient in a-Si:H was estimated using the CV and EIS methods. It equals  $4 \cdot 10^{-13} \text{ cm}^2/\text{s}$  for electrodes synthesized at a temperature of 100°C and  $10^{-13} \text{ cm}^2/\text{s}$  for those synthesized at a temperature of 250°C.

## ACKNOWLEDGEMENT

*This work was supported by the Russian Foundation for Basic Research, projects nos. 04-03-32034 and 05-08-18109.*

## List of symbols

|       |   |
|-------|---|
| $c$   | – concentration, mol dm <sup>-3</sup>       |
| $D$   | – diffusion coefficient, cm s <sup>-1</sup> |
| $E$   | – potential, mV, V                          |
| $F$   | – Faraday constant, C mol <sup>-1</sup>     |
| $f$   | – frequency, Hz                             |
| $I$   | – current, mA                               |
| $I_m$ | – mass current density, mA g <sup>-1</sup>  |
| $j$   | – current density                           |

- $n$  – charge  
 $Q$  – specific mass charge, C g<sup>-1</sup>  
 $R$  – resistance,  $\Omega$ , k $\Omega$   
 $T$  – temperature, °C  
 $t$  – time, s, min, h  
 $U$  – voltage, mV, V  
 $w$  – mass fraction  
 $\chi$  – number atoms  
 $Z$  – impedance,  $\Omega$   
 $\delta$  – thickness,  $\mu\text{m}$   
 $v$  – potential scan rate, mV s<sup>-1</sup>  
 $\rho$  – density, g cm<sup>-3</sup>  
 $\psi$  – volume ratio  
 $\sigma$  – conductivity, S cm<sup>-1</sup>

## References

- Besenhard J. O., Yang Y., Winter M., *J. Power Sources* **68** (1997) 87.
- Li H., Huang X. J., Chen L. Q., Zhou G. W., Zhang Z., Yu D. P., Mo Y. J., Pei N., *Solid State Ionics* **135** (2000) 181
- Jung Hunjoon, Park Min, Yoon Yeo-Geon, Kim Gi-Bum, Joo Seung-Ki, *J. Power Sources* **115** (2003) 346.
- Bourderau S., Brousse T., Schleich D. M., *J. Power Sources*, **81–82** (1999) 236
- Ohara S., Suzuki J., Sekine K., Takamura T., *J. Power Sources* **136** (2004) 303.
- Lee Ki-Lyoung, Jung Ju-Young, Lee Seung-Won, Moon Hee-Soo, Park Jong-Wan, *J. Power Sources* **130** (2004) 241.
- Lee Ki-Lyoung Jung, Ju-Young, Lee Seung-Won, Moon Hee-Soo, Park Jong-Wan, *J. Power Sources* **129** (2004) 270.
- Ohara S., Suzuki J., Sekine K., Takamura T., *J. Power Sources* **119–121** (2003) 591.
- Takamura T., Ohara S., Uehara M., Suzuki J., Sekine K., *J. Power Sources* **129** (2004) 96.
- Uehara M., Suzuki J., Tamura K., Sekine K., Takamura T., *J. Power Sources* **146** (2005) 441
- Yoshimura K., Suzuki J., Sekine K., Takamura T., *J. Power Sources* **146** (2005) 445.
- Graez C., Ahn C., Yazami R., Fultz B., *Electrochem. Solid State Lett.* **6** (2003) 194.
- Taeho Moon, Chunjoong Kim, Byungwoo Park, *J. Power Sources*, **155** (2006) 391.
- Borae Bang, Myung-Hoon Kim, Hee-Soo Moon, You-Kee Lee, Jong-Wan Park, *J. Power Sources*, **156** (2006) 604
- Park M. S., Wang G. X., Liu H. K., Dou. Ele S. X., *Electrochim. Acta*, **51** (2006) 5246
- Kon'kov O. I., Terukov E. I., Trapeznikova I. N., *Fiz. Tekhn. Poluprovod.* **30** (1996) 2183 (in Russian)
- Boukamp B. A., *Solid State Ionics* **20** (1986) 31.
- Zhang X.-W., Patil P. K., Wang Ch., Appleby A. J., Little, F. E. Cocke D. L., *J. Power Sources* **125** (2004) 206.
- Guo Z. P., Wang J. Z., Liu H. K., Dou S. X., *J. Power Sources* **146** (2005) 448
- Suzuki M., Suzuki J., Sekine K., Takamura T., *J. Power Sources* **146** (2005) 452
- Dimov N., Kugino S., Yoshio M., *Electrochim. Acta* **48** (2003) 1579.
- Dimov N., Fukuda K., Umeno T., Kugino S., Yoshio M., *J. Power Sources* **114** (2003) 88.
- de Levie R., *Electrochemical Responses of Porous and Rough Electrodes* in P. Delahay (ed.), *Advances in electrochemistry and electrochemical engineering*, N.-Y., Wiley, 1967, Vol. 6, p. 329–397.